High-order gravitational gradient effect in the gravity gradient measurement by the Eötvös-type torsion balance

Qi-Long Gong,[1] Yi-Xue Wang,[1,2] Lin Zhu,[1,*] Qi Liu,[3] and Cheng-Gang Shao[1]

[1] *MOE Key Laboratory of Fundamental Physical Quantities Measurement & Hubei Key Laboratory of Gravitation and Quantum Physics, PGMF and School of Physics, Huazhong University of Science and Technology, Wuhan 430074, People's Republic of China*

[2] *China Chang Jiang Energy Corporation, Wuhan 430205, People's Republic of China*

[3] *MOE Key Laboratory of TianQin Mission, TianQin Research Center for Gravitational Physics & School of Physics and Astronomy, Frontiers Science Center for TianQin, Gravitational Wave Research Center of CNSA, Sun Yat-sen University (Zhuhai Campus), Zhuhai 519082, People's Republic of China*

(Received 5 February 2024; accepted 11 April 2024; published 2 May 2024)

The Eötvös-type torsion balance is a well-known gravity gradient instrument for the regional or local geophysical exploration. As a key issue for the gravity gradient measurement, the estimation of the systematic effects in the instrument is rarely discussed as yet. This lack may lead to inconsistencies in the actual gravity gradient measurements. Among the systematic effects, one of the more obvious is the high-order gravitational gradient coupling, which is usually neglected in the measurement equation. This paper focuses on the estimation of such an effect. The coupling between the high-order gravitational gradient and the pendulum used in the instrument is charactered on the basis of the multipole expansion. It is presented that the coupling effect in the two versions of the commonly used Eötvös-type torsion balance can contribute a measurement bias of gravity gradient as large as approximately 20 E, approximately 10 E, respectively. The evaluation shows that the high-order gravitational gradient effect can not be ignored in the gravity gradient measurement by the Eötvös-type torsion balance. In addition, such an analysis method for the high-order gravitational gradient effect can also be applied to other types of gravity gradiometer or even gravimeters if required.

DOI: 10.1103/PhysRevApplied.21.054004

I. INTRODUCTION

Gravity gradient information has been widely applied in the fields, such as geological structure exploration [1], resource exploration [2], Earth gravity field inversion [3], and inertial navigation [4]. The most famous geodetic survey of gravity gradient may be traced back to the late 19th century. Loránd Eötvös introduced the torsion balance into the measurement of gravity gradient, and then built *curvature variometer* and *horizontal variometer*, now known as Eötvös torsion balance [5]. Subsequently, this geophysical instrument was improved and developed into different versions for oil and gas survey. More than 1 billion barrels of oil underground were detected, demonstrating the success of Eötvös-type torsion balance (ETB).

Unfortunately, the measurement by ETB is too time consuming mainly due to its long response time and static working mode. Since the 1950s, it has been gradually replaced by other instruments, such as the rotating differential accelerometers, superconducting sensors, and atomic interferometer [6]. Nonetheless, it is still the most precise gravity gradiometer with a relatively simple structure. It can achieve a precision of $\lesssim$1 E (1 E $= 10^{-9}$ m s^{-2}/m) level. Due to the high precision, it is now mainly used in the construction of standard gravity gradient fields or networks, and calibration of other types of gravity gradiometers. For example, Völgyesi *et al.* made the ETB reconstructed and modernized, and used it to measure the gravity gradients of gravity base points [7,8].

As a key issue in the gravity gradient measurements by ETB, the estimation of the systematic effects, which can contribute measurement bias is rarely discussed as yet. While the ETB is highly sensitive to environmental disturbances, including magnetic field and temperature temporal and spatial variations. Moreover, in the measurement equation of ETB, the high-order gravitational gradient (GG) terms are usually all ignored directly. These neglects seem unreasonable, and may lead to possible inconsistency in the actual gravity gradient measurements, which has been reported by Völgyesi *et al.* They measured the gravity gradient at different base points in a cave by employing one version of ETB, which encloses two antiparallel torsion balances so that two independent measurements can be completed simultaneously. It has been presented

*Corresponding author: zhulin36@mail.hust.edu.cn

that the two measurement results are not always consistent within the error range for different base points. The inconsistency can range from approximately 10 E to approximately 200 E [7], and suggests the possible existence of systematic effects. Consequently, the detailed estimation of these systematic effects in ETB seems inevitable and is also significant.

As an attempt, this paper describes the high-order GG effect in detail. Several concepts related to the gravity gradient are summarized in Sec. II. The measurement principle of the ETB is briefly reviewed in Sec. III. In Sec. IV, the multipole expansion method is exploited to depict the gravitation interaction between the pendulum and the surrounding mass source. The coupling of the high-order GG components to the pendulum is estimated in Sec. V.

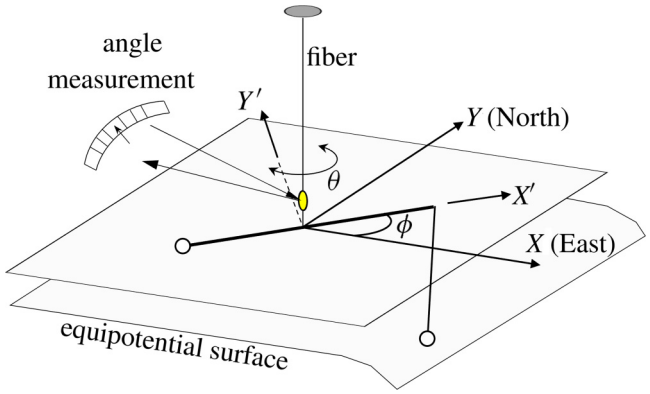

FIG. 1. Schematic drawing of the Eötvös-type torsion balance.

II. GRAVITY GRADIENT

The gravity potential $W(\vec{r})$ at a given point $\vec{r}$ due to the gravitation and rotation of the Earth can be written as

$$W(\vec{r}) = V(\vec{r}) + \Phi(\vec{r}), \tag{1}$$

where $V(\vec{r})$ is the gravitational potential, $\Phi(\vec{r})$ is the centrifugal potential. According to Newtonian law of gravitation, the gravitational potential can be expressed by

$$V(\vec{r}) = -\int \frac{G\,\mathrm{d}m_s}{|\vec{r}-\vec{r}_s|}, \tag{2}$$

where the integral covers the entire Earth with a mass distribution of $m_s(\vec{r}_s)$, G is the gravitational constant, $\vec{r}_s$ is the position vector of the mass element $\mathrm{d}m_s$.

If a Cartesian coordinate system is established, the gravity field $\vec{g}(\vec{r})$ can be defined by the gravity potential as

$$\vec{g}(x,y,z) = -\nabla W = -\nabla V - \nabla\Phi, \tag{3}$$

where gradient operator $\nabla = \left(\partial/\partial x, \partial/\partial y, \partial/\partial z\right)$. This definition has an extra negative sign "−" compared to that in Ref. [9].

The gravity gradient $[W_{ij}]$ $(i,j = x,y,z)$ at a certain position $\vec{r}_0$ is defined as the second-order derivative of the gravity potential, as

$$W_{ij}(\vec{r}_0) = \left.\frac{\partial^2 W}{\partial i \partial j}\right|_{\vec{r}=\vec{r}_0}. \tag{4}$$

In general, due to the differentiability of gravity potential $W(\vec{r})$, $[W_{ij}]$ is symmetric, $W_{xy} = W_{yx}$, $W_{xz} = W_{yz}$, and $W_{yz} = W_{yz}$, where $\vec{r}_0$ can be omitted if without ambiguity. For a local region, the gravity gradient is mainly contributed by the GG, which is determined by the local mass distribution. Curvature components W_{xy}, $W_\Delta = W_{yy} - W_{xx}$ can be used for the determination of local geoid forms. Horizontal components W_{xz}, W_{yz} can be employed to detect gravitation anomalies. Vertical component W_{zz} can be taken for the inversion reconstruction of the potential function.

III. MEASUREMENT PRINCIPLE OF THE EÖTVÖS-TYPE TORSION BALANCE

A. Principle of the Eötvös-type torsion balance

The ETB can measure horizontal and curvature components W_{zx}, W_{zy}, W_{xy}, and W_Δ. It mainly consists of a torsion pendulum and an angle-measuring unit, as shown in Fig. 1. The pendulum made up of a beam with two masses is suspended by a fiber, and can twist around the fiber. The deflecting angle θ is monitored by the angle-measuring unit.

The pendulum is assumed to only be subjected to the gravity and the tension from the fiber. At equilibrium, the fiber is straightened along the direction of local gravity. For description, a laboratory fixed frame $O-XYZ$ is established with the origin O at the center of mass of the pendulum, axis OZ upward along the direction of the fiber [10]. Axis OX and OY are both in the horizontal plane, say OX towards the east, and OY to the north then.

As the length dimension of the pendulum is far less than the radius of the Earth, the change in the centrifugal potential between two masses can be ignored, $\nabla\Phi = \vec{0}$. This means that the gravity gradient measured by the ETB is actually the GG. In order to calculate the torque applied on the pendulum due to the GG, the gravitational potential Eq. (2) need be further analyzed. Since the pendulum size scale is far smaller than the distance between the local mass source and the pendulum, the gravitational potential at the spatial location of the pendulum can be approximated by

Taylor expansion,

$$V(x,y,z) = V(\vec{0}) + \vec{r}\cdot\nabla V\big|_{\vec{r}=\vec{0}} + \left[\frac{1}{2!}(\vec{r}\cdot\nabla)^2 V\big|_{\vec{r}=\vec{0}}\right] + \text{high-order gravitational gradients}. \quad (5)$$

The third term on the right-hand side is related to the GG components. The fourth term—high-order GGs refers to the third or higher derivatives of the gravitational potential, like $V_{xxx} = \partial^3 V/\partial x^3\big|_{\vec{r}=\vec{0}}$. Clearly, the GG and high-order gradient components can be expressed as an integral only related to the mass distribution of the source mass (see Appendix B).

If the gravitation field generated by the local mass source is uniform, namely, the GG and high-order GGs in Eq. (5) are all zeros, the pendulum will not twist around the OZ axis for there is no gravitational torque. While the local gravitation field is not uniform, the pendulum will sense a torque around the OZ axis,

$$\tau_z = \int \left(\vec{r}\times\vec{g}(\vec{r})\right)\cdot\vec{e}_z\,\mathrm{d}m = -\int\left[\vec{r}\times\nabla V(\vec{r})\right]\cdot\vec{e}_z\,\mathrm{d}m, \quad (6)$$

where $\vec{e}_z$ is the unit vector of the OZ axis, $m(\vec{r})$ is the mass distribution of pendulum. If the high-order GGs are all ignored, the torque will become

$$\tau_z = V_{zx}(\vec{0})\int zy\,\mathrm{d}m - V_{zy}(\vec{0})\int xz\,\mathrm{d}m - V_{\Delta}(\vec{0})\int xy\,\mathrm{d}m - V_{xy}(\vec{0})\int (x^2-y^2)\,\mathrm{d}m. \quad (7)$$

The torque will twist the pendulum. Once the pendulum is at a different horizontal azimuth, the magnitude of τ_z will change due to the change in the mass distribution of the pendulum in the lab frame.

A body-fixed coordinate system $O'-X'Y'Z'$ is established for the pendulum. Axis $O'X'$ fixed with the pendulum decides the azimuth ϕ relative to axis OX. The $O'Z'$ axis coincides with OZ. Axis $O'Y'$ is perpendicular to the $X'O'Z'$ plane. For every point on the pendulum, the coordinates (x,y,z) in the lab frame can be transformed from (x',y',z') in the body-fixed frame by

$$\begin{bmatrix} x\\ y\\ z\end{bmatrix} = \begin{bmatrix}\cos\phi & -\sin\phi & 0\\ \sin\phi & \cos\phi & 0\\ 0 & 0 & 1\end{bmatrix}\begin{bmatrix} x'\\ y'\\ z'\end{bmatrix}. \quad (8)$$

Substituting Eq. (8) into Eq. (7), one can obtain the GG torque

$$\tau_z(\phi) = \begin{bmatrix} V_{zx} & V_{zy}\end{bmatrix}\left[\tilde{I}_{(1\phi)}\right]\begin{bmatrix}\sin(-\phi)\\ \cos(-\phi)\end{bmatrix} + \begin{bmatrix}\frac{1}{2}V_{\Delta} & -V_{xy}\end{bmatrix}\left[\tilde{I}_{(2\phi)}\right]\begin{bmatrix}\sin(-2\phi)\\ \cos(-2\phi)\end{bmatrix}, \quad (9)$$

where

$$\left[\tilde{I}_{(1\phi)}\right] = \begin{bmatrix}-\tilde{I}_{x'z'} & +\tilde{I}_{y'z'}\\ -\tilde{I}_{y'z'} & -\tilde{I}_{x'z'}\end{bmatrix},$$
$$\left[\tilde{I}_{(2\phi)}\right] = \begin{bmatrix}\tilde{I}_{x'x'}-\tilde{I}_{y'y'} & -2\tilde{I}_{x'y'}\\ 2\tilde{I}_{x'y'} & \tilde{I}_{x'x'}-\tilde{I}_{y'y'}\end{bmatrix}. \quad (10)$$

The component $\tilde{I}_{i'j'}$ $(i',j' = x',y',z')$ is defined by

$$\tilde{I}_{i'j'} = \int i'j'\,\mathrm{d}m. \quad (11)$$

In fact, $\tilde{I}_{i'j'}$ determines the sensing capability of the pendulum to the corresponding GG component.

The torque τ_z will cause the pendulum to twist until it balances with the elastic torque provided by the shear deformation of the suspension fiber at an angle of

$$\theta = n(\phi) - n_0 = \frac{\tau_z(\phi)}{k}, \quad (12)$$

where k is the torsional constant of the fiber. n_0 is the angle value with no GG torque when the pendulum locates in any azimuth, and usually cannot be read out directly. $n(\phi)$ is the angle reading with the GG components when the pendulum locates at azimuth ϕ. Equation (12) is called the measurement equation. It can be simplified to the general form in Ref. [9] with $\tilde{I}_{x'y'} = 0$, $\tilde{I}_{y'z'} = 0$.

IV. SPHERICAL MULTIPOLE EXPANSION

A. Spherical multipole expansion for the gravitational potential

From the perspective of multipole expansion, the analysis on the gravitational potential Eq. (5) is the multipole expansion in a Cartesian coordinate system. This approach has the drawback that it is complicated and difficult to determine the high-order GG terms [11]. In consideration of the rotary symmetry, multipole expansion in a spherical coordinate system is more suitable.

For the gravitational potential Eq. (2), as the distance between the source mass and origin O is always larger than that between the field point and O, namely $r_s > r$, the $1/|\vec{r}-\vec{r}_s|$ expression can be approximated by a series with spherical harmonics [12–14],

$$\frac{1}{|\vec{r}-\vec{r}_s|} = \sum_{\ell=0}^{\infty}\sum_{M=-\ell}^{\ell}\frac{4\pi}{2\ell+1}\left[r^{\ell}Y^*_{\ell M}(\theta,\varphi)\right]\left[\frac{Y_{\ell M}(\theta_s,\varphi_s)}{r_s^{\ell+1}}\right], \quad (13)$$

where (r,θ,φ), (r_s,θ_s,φ_s) are the spherical coordinates of vector $\vec{r}$ and $\vec{r}_s$, respectively, and "$*$" denotes the complex conjugate. The parameters in $Y_{\ell M}(\theta,\varphi)$, ℓ must be zero or a positive integer, and integer M can take only the values

$-\ell, -\ell+1, \cdots, 0, \cdots, \ell-1, \ell$. The spherical harmonics $Y_{\ell M}(\theta,\varphi)$ can be expressed as [12]

$$Y_{\ell M}(\theta,\varphi) = \sqrt{\frac{2\ell+1}{4\pi}\frac{(\ell-M)!}{(\ell+M)!}} P_\ell^M(\cos\theta) e^{\mathrm{i}M\varphi},$$

$P_\ell^M(\cos\theta)$ is associated Legendre polynomials,

$$P_\ell^M(\cos\theta) = \frac{(-1)^M}{2^\ell \ell!}(1-\cos^2\theta)^{\frac{M}{2}} \times \frac{\mathrm{d}^{\ell+M}}{\mathrm{d}(\cos\theta)^{\ell+M}}(\cos^2\theta-1)^\ell.$$

Substituting Eq. (13) into Eq. (2), one can get

$$V(\vec{r}) = -\sum_{\ell=0}^{\infty}\sum_{M=-\ell}^{\ell}\frac{4\pi G}{2\ell+1}\left[r^\ell Y_{\ell M}^*(\theta,\varphi)\right]Q_{\ell M}, \tag{14}$$

where

$$Q_{\ell M} = \int \frac{Y_{\ell M}(\theta_s,\varphi_s)}{r_s^{\ell+1}}\,\mathrm{d}m_s. \tag{15}$$

$Q_{\ell M}$ is an integral only related to the mass distribution of the local mass source. It describes the gravitation field generated by the local mass, and hence is called multipole field. As $Y_{\ell M}(\theta,\varphi)$ is a complex, $Q_{\ell M}$ is also a complex with a modulus $|Q_{\ell M}|$ and phase $\phi_{Q_{\ell M}}$,

$$Q_{\ell M} = |Q_{\ell M}|e^{\mathrm{i}\phi_{Q_{\ell M}}} = \mathrm{Re}[Q_{\ell M}] + \mathrm{i}\,\mathrm{Im}[Q_{\ell M}]. \tag{16}$$

$\mathrm{Re}[Q_{\ell M}]$ and $\mathrm{Im}[Q_{\ell M}]$ denote the real and imaginary parts of $Q_{\ell M}$, respectively.

The field component $Q_{\ell M}$ can more conveniently describe the GG and higher-order GG components, as presented in Appendix B. The GG components measured by the ETB have the relationships with the Q_{21} and Q_{22} fields, as

$$Q_{21} = \frac{1}{6G}\sqrt{\frac{15}{2\pi}}\left(V_{zx} + \mathrm{i}V_{zy}\right), \tag{17}$$

$$Q_{22} = \frac{1}{6G}\sqrt{\frac{15}{2\pi}}\left(\frac{1}{2}V_\Delta - \mathrm{i}V_{xy}\right). \tag{18}$$

B. Spherical multipole expansion on torque

The pendulum with a mass distribution $m(\vec{r})$ in the gravitational field characterized by the potential $V(\vec{r})$ can sense a torque τ_z as shown in Eq. (6). Clearly, the torque is related to the operator $\vec{r}\times\nabla$. This operator can be associated to the angular momentum operator in the quantum mechanics. It is defined by $\hat{L} \equiv -\mathrm{i}\hbar(\vec{r}\times\nabla)$ with the reduced Planck constant $\hbar$. The torque τ_z is related to the Cartesian component $\hat{L}_z$, which can be expressed in terms of spherical coordinates as (see Appendix C or Ref. [15])

$$\hat{L}_z = -\mathrm{i}\hbar(\vec{r}\times\nabla)\cdot\vec{e}_z = -\mathrm{i}\hbar\frac{\partial}{\partial\varphi}, \tag{19}$$

namely,

$$(\vec{r}\times\nabla)\cdot\vec{e}_z = \frac{\partial}{\partial\varphi}. \tag{20}$$

Hence the torque can be deduced [16] by

$$\tau_z = -\int\left[(\vec{r}\times\nabla)\cdot\vec{e}_z\right]V(\vec{r})\,\mathrm{d}m = -\int\frac{\partial}{\partial\varphi}V(\vec{r})\,\mathrm{d}m. \tag{21}$$

Expansion Eq. (14) is substituted into Eq. (21),

$$\tau_z = \sum_{\ell=0}^{\infty}\sum_{M=-\ell}^{\ell}\frac{4\pi G}{2\ell+1}Q_{\ell M}\int(-\mathrm{i}M)\left[r^\ell Y_{\ell M}^*(\theta,\varphi)\right]\mathrm{d}m, \tag{22}$$

where the minus "−" before "iM" is due to the derivative of the conjugate of spherical harmonics. In consideration of the rotary transformation between the lab frame and body-fixed frame,

$$r = r', \theta = \theta', \varphi = \varphi' + \phi,$$

resulting in the transformation of spherical harmonics

$$Y_{\ell M}(\theta,\varphi) = Y_{\ell M}(\theta',\varphi')e^{\mathrm{i}M\phi},$$

the torque τ_z can be rewritten as

$$\tau_z = \sum_{\ell=0}^{\infty}\sum_{M=-\ell}^{\ell}\frac{4\pi G}{2\ell+1}(-\mathrm{i}M)\,\tilde{q}_{\ell M}\,Q_{\ell M}\,e^{-\mathrm{i}M\phi}, \tag{23}$$

where

$$\tilde{q}_{\ell M} = \int r'^\ell Y_{\ell M}^*(\theta',\varphi')\,\mathrm{d}m. \tag{24}$$

Such an integral is only related to the mass distribution of pendulum in the body-fixed frame, and called mass multipole moment of the pendulum. Naturally, the moment $\tilde{q}_{\ell M}$ describes the sensitivity of the pendulum to the GG or high-order GG component, as shown in Appendix B.

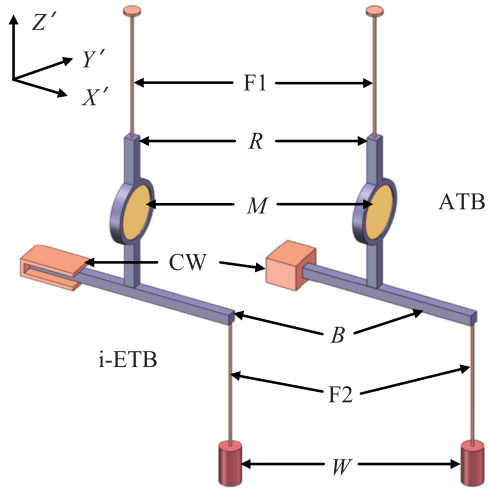

FIG. 2. Schematic drawing of two pendulums used in i-ETB and ATB (drawing not to scale). F1, the suspension fiber; *B*, beam; F2, fiber hanging the counterweight; *W*, weight; CW, counterweight; *R*, rod; *M*, mirror. The shape of counterweight component is different for two pendulums.

The moment $\tilde{q}_{21}$ and $\tilde{q}_{22}$ components have the relationships between the mass quadrupole moment components $\tilde{I}_{ij}$, as

$$\tilde{q}_{21} = -\frac{1}{2}\sqrt{\frac{15}{2\pi}}\left(\tilde{I}_{x'z'} - \mathrm{i}\tilde{I}_{y'z'}\right), \tag{25}$$

$$\tilde{q}_{22} = \frac{1}{2}\sqrt{\frac{15}{2\pi}}\left[\frac{1}{2}\left(I_{x'x'} - I_{y'y'}\right) - \mathrm{i}I_{x'y'}\right]. \tag{26}$$

By further simplification as shown in Appendix D, torque Eq. (23) can be expressed by

$$\tau_z(\phi) = \sum_{\ell=2}^{\infty}\sum_{M=1}^{\ell}\frac{8\pi MG}{2\ell+1}\left[\mathrm{Re}[Q_{\ell M}] \quad \mathrm{Im}[Q_{\ell M}]\right] \times \left[\tilde{q}_{(M\phi)}\right]\begin{bmatrix}\sin(-M\phi)\\ \cos(-M\phi)\end{bmatrix}, \tag{27}$$

where

$$\left[\tilde{q}_{(M\phi)}\right] = \begin{bmatrix}|\tilde{q}_{\ell M}|\cos\phi_{\tilde{q}_{\ell M}} & |\tilde{q}_{\ell M}|\sin\phi_{\tilde{q}_{\ell M}}\\ -|\tilde{q}_{\ell M}|\sin\phi_{\tilde{q}_{\ell M}} & |\tilde{q}_{\ell M}|\cos\phi_{\tilde{q}_{\ell M}}\end{bmatrix}.$$

The summation about M from $M = -\ell$ to ℓ has been transformed from $M = 1$ to ℓ. Since the center of mass of the pendulum is defined as the origin, the term q_{11} naturally vanishes. $|\tilde{q}_{\ell M}|$, $\phi_{\tilde{q}_{\ell M}}$ are the modulus and phase of $\tilde{q}_{\ell M}$, respectively.

Expression Eq. (27) completely describes all terms including the high-order GG components. The term with

TABLE I. The mass distribution of the two pendulums.

	Shape (cm)	Dimensions	Geometric center (x', y', z') (cm)	Density (g/cm^3)
B[a]	Cuboid	$40.0 \times 0.4 \times 0.4$	(0.0, 0.0, 0.0)	2.7
	Cuboid	$14.0 \times 0.4 \times 0.4$	(0.0, 0.0, 0.0)	2.7
CW	U shaped	$8.5 \times 1.2 \times 0.2$	(−18.1, 0.0, 0.0)	19.6
	Cuboid	$1.0 \times 1.2 \times 1.5$	(−6.4, 0.0, 0.0)	8.9
W	Cylinder	$\Phi 0.8 \times 2.7$	(20.0, 0.0, −64.5)	19.6
	Cylinder	$\Phi 0.8 \times 1.4$	(6.6, 0.0, −20.9)	19.6
M	Cylinder	$\Phi 2.0 \times 0.3$	(0.0, 0.0, 4.7)	2.2
	Cylinder	$\Phi 2.0 \times 0.3$	(0.0, 0.0, 3.0)	2.2
R	Cuboid	$0.4 \times 0.4 \times 10.0$	(0.0, 0.0, 5.2)	2.7
	Cuboid	$0.4 \times 0.4 \times 6.0$	(0.0, 0.0, 3.0)	2.7

[a]The upper line is for the i-ETB pendulum, the lower for the ATB pendulum, the same below.

$\ell = 2$, $M = 1$ corresponds to the coupling of the V_{zx} and V_{zy} components to the pendulum. The term with $\ell = 2$, $M = 2$ corresponds to the coupling with V_Δ and V_{xy}. These two terms are exactly what has been described above in Eq. (9). The terms with $\ell \geqslant 3$ are the coupling to the high-order GG components.

According to Eq. (27), the torque τ_z is a Fourier series about the azimuth ϕ. For a given value of M, the coefficients of $\sin(-M\phi)$ and $\cos(-M\phi)$ can be expressed by

$$\tau_{z,\sin}^{(M\phi)} = \sum_{\ell=2}^{\infty}\frac{8\pi MG}{2\ell+1} \times \left(\mathrm{Re}[Q_{\ell M}]\mathrm{Re}[\tilde{q}_{\ell M}] - \mathrm{Im}[Q_{\ell M}]\mathrm{Im}[\tilde{q}_{\ell M}]\right), \tag{28}$$

$$\tau_{z,\cos}^{(M\phi)} = \sum_{\ell=2}^{\infty}\frac{8\pi MG}{2\ell+1} \times \left(\mathrm{Re}[Q_{\ell M}]\mathrm{Im}[\tilde{q}_{\ell M}] + \mathrm{Im}[Q_{\ell M}]\mathrm{Re}[\tilde{q}_{\ell M}]\right), \tag{29}$$

respectively. For the terms with $M = 1$, $\tau_{z,\sin}^{(1\phi)}$ and $\tau_{z,\cos}^{(1\phi)}$ include not only the contribution of Q_{21} field or GG horizontal components, but also the coupling of high-order GG components like $Q_{31}, Q_{41}, \cdots$, fields. For $M = 2$, $\tau_{z,\sin}^{(2\phi)}$ and $\tau_{z,\cos}^{(2\phi)}$ include the coupling with not only the Q_{22} field or GG curvature components, but also the $Q_{32}, Q_{42}, \cdots$, fields.

It can be concluded that the magnitude of any term in the series Eq. (28) or Eq. (29) is proportional to the product $|\tilde{q}_{\ell M}||Q_{\ell M}|$, hence series Eqs. (28) and (29) are both convergent. The convergence factor is r_0/R_0, where r_0 and R_0 are typical values of the pendulum dimension and the distance between the local source mass and the pendulum,

respectively. Therefore, for a specific measurement with an expected accuracy, not all terms need to be considered. The expected accuracy determines the truncation term in the series Eqs. (28) and (29). For example, if $r_0 \sim 0.2$ m and $R_0 \gtrsim 2$ m, the convergence factor $r_0/R_0 \lesssim 0.1$, representing the coupling $|\tilde{q}_{41}||Q_{41}|$ is $(R_0/r_0)^{4-2} \gtrsim 100$ times weaker than the coupling $|\tilde{q}_{21}||Q_{21}|$ if the pendulum was not specially designed. In other words, for the gravity gradient measurement by the ETB, if the desired relative accuracy is about 1%, what should be investigated is the coupling terms $|\tilde{q}_{3M}||Q_{3M}|$, $|\tilde{q}_{4M}||Q_{4M}|$, and $|\tilde{q}_{5M}||Q_{5M}|$ with $M = 1, 2$.

V. HIGH-ORDER GRAVITATIONAL GRADIENT EFFECT

A. Estimation of multipole moment of the pendulum

Due to the neglect of the high-order GG coupling in the ETB, the pendulum is designed without consideration of the sensitivity to the high-order GG component. This may lead to relatively large $|\tilde{q}_{\ell M}|$ ($\ell = 3, 4, 5; M = 1, 2$). As an example, here we analyze the pendulums in two versions of ETB, the initial ETB (i-ETB) and Auterbal torsion balance (ATB). The latter is used in the measurement by Völgyesi *et al.* [7]. Their main structures are similar, including a beam (B), a weight (W), a counterweight (CW), a mirror (M) and a rod (R), respectively, as shown in Fig. 2.

It is difficult to collect complete information on the mass distribution of the two pendulums. Without affecting the conclusion, their mass distribution are both simply modeled according to Refs. [5,9]. The density of each component are assumed to be uniform. Table I lists the mass distribution of the two pendulums in the body-fixed frame.

The multipole moments $\tilde{q}_{\ell M}(\ell \leq 5, M \leq 2)$ by each component of two pendulums are then calculated, as shown in Tables II and III. The results show that it is the component—weight—that plays a leading role in $\tilde{q}_{\ell M}$ of each pendulum. The moment components $\tilde{q}_{\ell M}$ in the ATB are all smaller than those in the i-ETB, as the ATB pendulum is reduced in dimensions compared to the i-ETB one.

B. Evaluation of the high-order gravitational gradient

In order to estimate the torque component by the coupling of $Q_{\ell M}$ ($\ell = 3, 4, 5; M = 1, 2$) in the measurement by ETB, the typical values of $Q_{\ell M}$ should be input. These values could be evaluated by calculating the integral Eq. (15) with constructed mass distribution of the local source, or measured by designing different pendulums to be sensitive to each component. Here the typical values of the

TABLE II. The multipole moment $\tilde{q}_{\ell M}$ by each component of the pendulum in the i-ETB.

	Component	$\tilde{q}_{\ell 1}$	$\tilde{q}_{\ell 2}$	Unit
$\ell = 2$	B	0.0	0.9×10^{-4}	kg m^2
	CW	0.0	3.8×10^{-4}	
	W	2.7×10^{-3}	4.0×10^{-4}	
	M	$<10^{-6}$	$<10^{-7}$	
	R	0.0	0.0	
	total	2.7×10^{-3}	8.8×10^{-4}	kg m^2
$\ell = 3$	B	0.0	0.0	kg m^3
	CW	-0.06×10^{-3}	0.0	
	W	-2.8×10^{-3}	-7.0×10^{-4}	
	M	0.0	0.0	
	R	0.0	0.0	
	total	-2.9×10^{-3}	-7.0×10^{-4}	kg m^3
$\ell = 4$	B	0.0	-0.1×10^{-5}	kg m^4
	CW	0.0	-1.1×10^{-5}	
	W	2.6×10^{-3}	8.8×10^{-4}	
	M	0.0	0.0	
	R	0.0	0.0	
	total	2.6×10^{-3}	8.7×10^{-4}	kg m^4
$\ell = 5$	B	0.0	0.0	kg m^5
	CW	2.0×10^{-6}	0.0	
	W	-2.1×10^{-3}	-9.4×10^{-4}	
	M	0.0	0.0	
	R	0.0	0.0	
	total	-2.1×10^{-3}	-9.4×10^{-4}	kg m^5

TABLE III. The multipole moment $\tilde{q}_{\ell M}$ by each component of the pendulum in the ATB.

	Component	$\tilde{q}_{\ell 1}$	$\tilde{q}_{\ell 2}$	Unit
$\ell = 2$	B	0.0	0.4×10^{-5}	kg m^2
	CW	0.0	2.3×10^{-5}	
	W	1.5×10^{-4}	2.3×10^{-5}	
	M	0.0	$<10^{-7}$	
	R	0.0	0.0	
	total	1.5×10^{-4}	5.0×10^{-5}	kg m^2
$\ell = 3$	B	0.0	0.0	kg m^3
	CW	-0.1×10^{-5}	0.0	
	W	-5.0×10^{-5}	-1.3×10^{-5}	
	M	0.0	0.0	
	R	0.0	0.0	
	total	-5.1×10^{-5}	-1.3×10^{-5}	kg m^3
$\ell = 4$	B	0.0	-9.7×10^{-9}	kg m^4
	CW	0.0	-8.1×10^{-8}	
	W	1.5×10^{-5}	5.2×10^{-6}	
	M	0.0	0.0	
	R	0.0	0.0	
	total	1.5×10^{-5}	5.1×10^{-6}	kg m^4
$\ell = 5$	B	0.0	0.0	kg m^5
	CW	5.0×10^{-9}	0.0	
	W	-3.8×10^{-6}	-1.8×10^{-6}	
	M	0.0	0.0	
	R	0.0	0.0	
	total	-3.8×10^{-6}	-1.8×10^{-6}	kg m^5

TABLE IV. The calculated values of Q_{lm} from Eöt-Wash group, data from Table 6.7 in Ref. [17].

	$Q_{\ell 1}$	$Q_{\ell 2}$	Unit
$\ell = 3$	$(0.1 + 1.1\,\mathrm{i}) \times 10^2$	$(0.2 + 1.3\,\mathrm{i}) \times 10^2$	$\mathrm{kg \cdot m^{-4}}$
$\ell = 4$	$(-0.6 - 9.6\,\mathrm{i}) \times 10^1$	$(0.1 + 1.5\,\mathrm{i}) \times 10^1$	$\mathrm{kg \cdot m^{-5}}$
$\ell = 5$	$(-0.3 - 5.5\,\mathrm{i}) \times 10^2$	$(-0.4 - 3.1\,\mathrm{i}) \times 10^2$	$\mathrm{kg \cdot m^{-6}}$

field components are taken into the calculated values in the test of the equivalence principle by the Eöt-Wash group [17], as listed in Table IV. In the equivalence-principle test with a high precision, they calculated the multipole field components by modeling the local mass distribution for the surrounding area with a radius of approximately 60 m. To accurately evaluate the gravitational correction on the equivalence-principle violating signal, they also measured the Q_{21}, Q_{31}, and Q_{41} components. The measurement shows that the measured values agree with the calculated in order of magnitude. Similar measurements has been also completed by another group [18]. Their measurement results of Q_{21}, Q_{31}, and Q_{41} are close in magnitude to those of the Eöt-Wash group, respectively. This consistency suggests that if there are no gravitation anomalies, each multipole field component for different indoor sites should have similar magnitudes. It should be noted that the actual values of each component $Q_{\ell M}$ at a site may differ from these values. For the locations with gravity anomalies, such as near the entrance of a cave, the difference may be even greater.

C. Evaluation of high-order gravitational gradient effect

For estimation, all the typical values of the measured GG components by the ETB are taken here simply as 100 E, namely, $V_{zx} \simeq 100$ E, $V_{zy} \simeq 100$ E, $V_{xy} \simeq 100$ E, and $V_\Delta \simeq 100$ E. Correspondingly, the multipole field components $Q_{21} \simeq (3.9 + 3.9\,\mathrm{i}) \times 10^2\ \mathrm{kg\,m^{-3}}$, $Q_{22} \simeq (1.9 - 3.9\,\mathrm{i}) \times 10^2\ \mathrm{kg\,m^{-3}}$. The coupling of field Q_{21} to the moment $\tilde{q}_{21}$ of the i-ETB pendulum will contribute to a torque with $\sin(-\phi)$ and $\cos(-\phi)$ components of 3.5×10^{-10} N m and 3.5×10^{-10} N m, respectively.

TABLE V. The estimated component of torque generated by each GG and high-order GG component in the i-ETB, unit: 10^{-10} N m.

	$\tau^{(1\phi)}_{z,\sin}$	$\tau^{(1\phi)}_{z,\cos}$	$\tau^{(2\phi)}_{z,\sin}$	$\tau^{(2\phi)}_{z,\cos}$
$\ell = 2$	3.5	3.5	1.1	−2.3
$\ell = 3$	−0.07	−0.76	−0.07	−0.43
$\ell = 4$	−0.03	−0.46	0.00	0.06
$\ell = 5$	0.10	1.80	0.11	0.89
subtotal[a]	0.00	0.58	0.04	0.52

[a]Summation of high-order terms from $\ell = 3$ to $\ell = 5$.

TABLE VI. The estimated component of torque generated by each GG and high-order GG component in the ATB, unit: 10^{-12} N m.

	$\tau^{(1\phi)}_{z,\sin}$	$\tau^{(1\phi)}_{z,\cos}$	$\tau^{(2\phi)}_{z,\sin}$	$\tau^{(2\phi)}_{z,\cos}$
$\ell = 2$	19.6	19.6	6.4	−13.1
$\ell = 3$	−0.12	−1.34	−0.12	−0.81
$\ell = 4$	−0.02	−0.27	0.00	0.03
$\ell = 5$	0.02	0.32	0.02	0.17
subtotal[a]	−0.12	−1.29	−0.10	−0.61

[a]Summation of high-order terms from $\ell = 3$ to $\ell = 5$.

The $\tilde{q}_{22}Q_{22}$ coupling will contribute the $\sin(-2\phi)$ and $\cos(-2\phi)$ components of 1.1×10^{-10} N m and -2.3×10^{-10} N m, respectively.

After entering values of the mass-moment components $\tilde{q}_{\ell M}$ and field components $Q_{\ell M}$, we can evaluate the torque by Eq. (27). The torque component due to each high-order GG component in i-ETB and ATB is shown in Tables V and VI, respectively.

For the GG measurements by the i-ETB and ATB, it is now assumed that each measured torque component is the value only due to each typical GG component. If all high-order GG components are ignored, the measurement equation will give each typical value of the GG. But if the high-order GG components cannot be neglected, each measured GG component will differ. The high-order GG coupling will contribute measurement bias and should be corrected. The corrected values are shown in Table VII.

Table VII shows that the high-order GG terms can contribute a measurement bias with about approximately 20 E or approximately 10 E in several GG components by i-ETB or ATB. For an actual measurement site, especially the transition zone between indoors and outdoors like the entrance of a cave, the high-order GG components may be larger than the typical values in Table IV. The closer to the transition zone, the more significant the high-order GG effect. This trend was also observed in the ATB measurement by Völgyesi *et al*. If each multipole field component

TABLE VII. The difference of gravity gradients with and without considering the high-order GG for typical gravity gradient with 100 E, unit: E.

	Without[a]	With[b]		Difference[c]	
W_{zx}	100	100	102	0	2
W_{zy}	100	84	108	−16	8
W_Δ	100	93	100	−7	0
W_{xy}	100	124	96	24	−4

[a]Disregarding the high-order GG terms.
[b]Considering the high-order GG terms, the left is for the i-ETB, right is ATB.
[c]Compared to the typical value.

$Q_{\ell M}$ is 5 times or even more larger than the typical value near the the entrance of a cave, the difference may reach 50 E or more.

VI. CONCLUSIONS AND DISCUSSION

In summary, the high-order GG coupling in the gravity gradient measurement by the ETB is discussed in detail. The torque sensed by the pendulum in a gravitation field due to the local mass source can be expressed via multipole expansion. The gravitation field at the spatial location of the pendulum can be described by the multipole field, which is an integral only related to the mass distribution of local source. The sensitivity of pendulum to each multipole field component is determined by the mass multipole moment, which is also an integral only related to the mass distribution of the pendulum. By calculating the mass multipole moment of the pendulum and inputting the typical values of the high-order GG, we can conclude that the high-order GG effect can contribute a measurement bias of approximately 10 E at least, and thus is a significant systematic effect in the ETB.

If the GG was measured accurately by the ETB, the current pendulum should be further optimized as it has large $\tilde{q}_{\ell 1}$ and $\tilde{q}_{\ell 2}$ ($\ell = 3, 4, \ldots$). This optimization can be achieved either by further reducing the length dimension of the pendulum or by adjusting the mass distribution of the pendulum. In addition, other systematic effects in the ETB, such as magnetic and thermal coupling, need to be evaluated carefully.

If the high-order GG effect contributes a non-negligible correction in other type gravity gradiometers or even gravimeters including absolute and relative types, the above analysis could be employed.

ACKNOWLEDGMENTS

This work is supported by the National Key R&D Program of China (Grant No. 2023YFC2206300 and Task No. 2022YFC2204101), and the National Natural Science Foundation of China (Grants No. 12005308 and No. 12150012).

APPENDIX A: SPHERICAL HARMONICS IN CARTESIAN COORDINATES

The spherical harmonics is usually presented in the form of spherical coordinates, as

$$Y_{\ell M}(\theta,\varphi) = \sqrt{\frac{2\ell+1}{4\pi}\frac{(\ell-M)!}{(\ell+M)!}} P_\ell^M(\cos\theta) e^{\mathrm{i}M\varphi}, \quad \text{(A1)}$$

where $P_\ell^M(\cos\theta)$ is associated Legendre polynomials,

$$P_\ell^M(\cos\theta) = \frac{(-1)^M}{2^\ell \ell!}(1-\cos^2\theta)^{M/2} \times \frac{\mathrm{d}^{\ell+M}}{\mathrm{d}(\cos\theta)^{\ell+M}}(\cos^2\theta - 1)^\ell.$$

For a vector $\vec{r}$, the relationships between the Cartesian coordinates (x, y, z) and spherical coordinates (r, θ, φ) are

$$x = r\sin\theta\cos\varphi, \quad \text{(A2)}$$

$$y = r\sin\theta\sin\varphi, \quad \text{(A3)}$$

$$z = r\cos\theta. \quad \text{(A4)}$$

The above Eqs. (A2)–(A4) can be substituted into Eq. (A1), and the spherical harmonics will be expressed in the form of Cartesian coordinates then. For example, for Y_{21},

$$Y_{21}(\theta,\varphi) = -\frac{1}{2}\sqrt{\frac{15}{2\pi}}\sin\theta\cos\theta e^{\mathrm{i}\varphi} \quad \text{(A5)}$$

$$= -\frac{1}{2}\sqrt{\frac{15}{2\pi}}\frac{r\sin\theta}{r}\frac{r\cos\theta}{r}(\cos\varphi + \mathrm{i}\sin\varphi)$$

$$= -\frac{1}{2}\sqrt{\frac{15}{2\pi}}\frac{z(x+\mathrm{i}y)}{r^2}. \quad \text{(A6)}$$

Other spherical harmonics terms can be obtained in a similar way. Table VIII lists the terms with $\ell = 1, 2, 3, 4$; $M = 0, 1, 2$.

TABLE VIII. The spherical harmonics with with $\ell = 1, 2, 3, 4$; $M = 0, 1, 2$.

	$M=0$	$M=1$	$M=2$
$\ell=1$	$\frac{1}{2}\sqrt{\frac{3}{\pi}}\cdot\frac{z}{r}$	$-\frac{1}{2}\sqrt{\frac{3}{2\pi}}\frac{(x+iy)}{r}$	$\cdots$
$\ell=2$	$\frac{1}{4}\sqrt{\frac{5}{\pi}}\frac{3z^2-r^2}{r^2}$	$-\frac{1}{2}\sqrt{\frac{15}{2\pi}}\frac{z(x+\mathrm{i}y)}{r^2}$	$\frac{1}{4}\sqrt{\frac{15}{2\pi}}\frac{(x+\mathrm{i}y)^2}{r^2}$
$\ell=3$	$\frac{1}{4}\sqrt{\frac{7}{\pi}}\frac{5z^3-3zr^2}{r^3}$	$-\frac{1}{8}\sqrt{\frac{21}{\pi}}\frac{(5z^2-r^2)(x+\mathrm{i}y)}{r^3}$	$\frac{1}{4}\sqrt{\frac{105}{2\pi}}\frac{(x+\mathrm{i}y)^2 z}{r^3}$
$\ell=4$	$\frac{3}{16}\sqrt{\frac{1}{\pi}}\frac{(35z^4-30z^2r^2+3r^4)}{r^4}$	$-\frac{3}{8}\sqrt{\frac{5}{\pi}}\frac{(x+\mathrm{i}y)(7z^3-3zr^2)}{r^4}$	$\frac{3}{8}\sqrt{\frac{5}{2\pi}}\frac{(x+\mathrm{i}y)^2(7z^2-r^2)}{r^4}$

APPENDIX B: RELATIONSHIP BETWEEN GRAVITATIONAL GRADIENT AND MULTIPOLE FIELD

According to the definition, the GG component, say curvature component V_{xx}, due to the local source with a mass distribution of $m_s(\vec{r}_s)$, can be written as

$$V_{xx} = \left.\frac{\partial^2 V}{\partial x^2}\right|_{\vec{r}=\vec{0}} \tag{B1}$$

$$= \left[\frac{\partial^2}{\partial x^2}\left(-\int \frac{G\,\mathrm{d}m_s}{|\vec{r}-\vec{r}_s|}\right)\right]\Bigg|_{\vec{r}=\vec{0}}$$

$$= -G\int \left[\frac{\partial^2}{\partial x^2}\left(\frac{1}{|\vec{r}-\vec{r}_s|}\right)\right]\Bigg|_{\vec{r}=\vec{0}} \mathrm{d}m_s$$

$$= G\int \frac{y_s^2+z_s^2-2x_s^2}{r_s^5}\,\mathrm{d}m_s. \tag{B2}$$

Likewise, other GG components can also deduced as

$$V_{yy} = G\int \frac{x_s^2+z_s^2-2y_s^2}{r_s^5}\mathrm{d}m_s, \tag{B3}$$

$$V_{zz} = G\int \frac{x_s^2+y_s^2-2z_s^2}{r_s^5}\,\mathrm{d}m_s, \tag{B4}$$

and

$$V_{xy} = V_{yx} = G\int \frac{-3x_sy_s}{r_s^5}\,\mathrm{d}m_s, \tag{B5}$$

$$V_{xz} = V_{zx} = G\int \frac{-3x_sz_s}{r_s^5}\,\mathrm{d}m_s, \tag{B6}$$

$$V_{yz} = V_{zy} = G\int \frac{-3y_sz_s}{r_s^5}\,\mathrm{d}m_s. \tag{B7}$$

From the expressions of V_{xx}, V_{yy}, and V_{zz}, one can get

$$V_{xx}+V_{yy}+V_{zz} = 0. \tag{B8}$$

Substituting the expressions of spherical harmonics in Cartesian coordinates into $Q_{\ell M}$, we can get the specific formula of $Q_{\ell M}$. For example, for Q_{22} of interest,

$$Q_{22} = \int \frac{Y_{22}(\theta_s,\varphi_s)}{r_s^3}\,\mathrm{d}m_s \tag{B9}$$

$$= \frac{1}{4}\sqrt{\frac{15}{2\pi}}\int \frac{(x_s^2-y_s^2)+\mathrm{i}(2x_sy_s)}{r_s^5}\mathrm{d}m_s, \tag{B10}$$

and for Q_{21} and Q_{20},

$$Q_{21} = \frac{1}{2}\sqrt{\frac{15}{2\pi}}\int \frac{-x_sz_s-\mathrm{i}(y_sz_s)}{r_s^5}\mathrm{d}m_s, \tag{B11}$$

$$Q_{20} = \frac{1}{4}\sqrt{\frac{15}{2\pi}}\int \frac{-(x_s^2+y_s^2-2z_s^2)}{r_s^5}\mathrm{d}m_s. \tag{B12}$$

Comparing the equations for the GG components and multipole field Q_{2M} components, we can obtain the relationship between them. For Q_{22} component,

$$Q_{22} = \frac{1}{4}\sqrt{\frac{15}{2\pi}}\int \frac{(x_s^2-y_s^2)+\mathrm{i}(2x_sy_s)}{r_s^5}\mathrm{d}m_s$$

$$= \frac{1}{4}\sqrt{\frac{15}{2\pi}}\left[\int \frac{x_s^2-y_s^2}{r_s^5}\mathrm{d}m_s + \int \frac{\mathrm{i}(2x_sy_s)}{r_s^5}\mathrm{d}m_s\right]$$

$$= \frac{1}{4}\sqrt{\frac{15}{2\pi}}\left(\frac{V_{yy}-V_{xx}}{3G}+\mathrm{i}\frac{-2V_{xy}}{3G}\right)$$

$$= \frac{1}{6G}\sqrt{\frac{15}{2\pi}}\left(\frac{V_\Delta}{2}-\mathrm{i}\,V_{xy}\right), \tag{B13}$$

and for Q_{21} and Q_{20},

$$Q_{21} = \frac{1}{6G}\sqrt{\frac{15}{2\pi}}\left(V_{zx}+\mathrm{i}\,V_{zy}\right), \tag{B14}$$

$$Q_{20} = -\frac{1}{12G}\sqrt{\frac{15}{2\pi}}V_{zz}. \tag{B15}$$

Similarly, it can be inferred that there is relationship between high-order GG components and $Q_{\ell M}$. For example, for Q_{3M},

$$Q_{30} = -\frac{1}{12G}\sqrt{\frac{7}{\pi}}V_{zzz}, \tag{B16}$$

$$Q_{31} = \frac{1}{24G}\sqrt{\frac{21}{\pi}}\left(V_{xzz}+\mathrm{i}V_{yzz}\right), \tag{B17}$$

$$Q_{32} = -\frac{1}{30G}\sqrt{\frac{105}{2\pi}}\left[(V_{xxz}+\frac{1}{2}V_{zzz})+\mathrm{i}V_{xyz}\right], \tag{B18}$$

$$Q_{33} = \frac{1}{120G}\sqrt{\frac{35}{\pi}}\left[(V_{xxx}-3V_{xyy})-\mathrm{i}(V_{yyy}-3V_{xxy})\right]. \tag{B19}$$

It is noted that the above combinations are not unique since one can use the equations deduced from Eq. (B8), like

$$V_{zzz} = -V_{zxx}-V_{zyy}. \tag{B20}$$

APPENDIX C: DEDUCTION OF OPERATOR $\vec{r}\times\nabla$

The angular momentum operator in quantum mechanics is

$$\hat{L} = \vec{r}\times\hat{p} = \vec{r}\times(-\mathrm{i}\hbar\nabla) = -\mathrm{i}\hbar\left(\vec{r}\times\nabla\right),$$

where $\hbar$ is the reduced Planck constant. The z component of $\hat{L}$ is

$$\hat{L}_z = \hat{L}\cdot\vec{e}_z = -\mathrm{i}\hbar\left(\vec{r}\times\nabla\right)\cdot\vec{e}_z \tag{C1}$$

$$= -\mathrm{i}\hbar\left(x\frac{\partial}{\partial y}-y\frac{\partial}{\partial x}\right). \tag{C2}$$

It consists of two operators, $\partial/\partial x$ and $\partial/\partial y$. The operator $\partial/\partial x$ can be transformed to spherical coordinates,

$$\frac{\partial}{\partial x} = \frac{\partial r}{\partial x}\frac{\partial}{\partial r} + \frac{\partial \theta}{\partial x}\frac{\partial}{\partial \theta} + \frac{\partial \varphi}{\partial x}\frac{\partial}{\partial \varphi}. \tag{C3}$$

Taking into account the relationship between Cartesian and spherical coordinate, one can get the partial derivatives, including $\partial\alpha/\partial x$ ($\alpha = r, \theta, \varphi$). For $\partial r/\partial x$,

$$\frac{\partial r}{\partial x} = \frac{\partial}{\partial x}\left(\sqrt{x^2+y^2+z^2}\right) = \frac{x}{r} = \sin\theta\cos\varphi. \tag{C4}$$

For $\partial\theta/\partial x$,

$$\begin{aligned}\frac{\partial \theta}{\partial x} &= \frac{\mathrm{d}\theta}{\mathrm{d}(\cos\theta)}\frac{\partial(\cos\theta)}{\partial x} = -\frac{1}{\sin\theta}\frac{\partial(\cos\theta)}{\partial x} \\ &= -\frac{1}{\sin\theta}\frac{\partial}{\partial x}\left(\frac{z}{r}\right) = \frac{\cos\theta\cos\varphi}{r}.\end{aligned} \tag{C5}$$

For $\partial\varphi/\partial x$,

$$\begin{aligned}\frac{\partial \varphi}{\partial x} &= \frac{\mathrm{d}\varphi}{\mathrm{d}(\tan\varphi)}\frac{\partial(\tan\varphi)}{\partial x} = \cos^2\varphi\frac{\partial(\tan\varphi)}{\partial x} \\ &= \cos^2\varphi\frac{\partial}{\partial x}\left(\frac{y}{x}\right) = -\frac{\sin\varphi}{r\sin\theta}.\end{aligned} \tag{C6}$$

Substituting the above equations into Eq. (C3), we can obtain

$$\frac{\partial}{\partial x} = \sin\theta\cos\varphi\frac{\partial}{\partial r} + \frac{\cos\theta\cos\varphi}{r}\frac{\partial}{\partial\theta} - \frac{\sin\varphi}{r\sin\theta}\frac{\partial}{\partial\varphi}. \tag{C7}$$

Likewise, the operation $\partial/\partial y$ can be transformed to

$$\frac{\partial}{\partial y} = \sin\theta\sin\varphi\frac{\partial}{\partial r} + \frac{\cos\theta\sin\varphi}{r}\frac{\partial}{\partial\theta} + \frac{\cos\varphi}{r\sin\theta}\frac{\partial}{\partial\varphi}. \tag{C8}$$

Substituting Eqs. (A2)–(A4), (C7), and (C8) into Eq. (C2), the operator $\hat{L}_z$ can be rewritten as

$$\hat{L}_z = -\mathrm{i}\hbar\frac{\partial}{\partial\varphi}, \tag{C9}$$

namely,

$$\left(\vec{r}\times\nabla\right)\cdot\vec{e}_z = \left(x\frac{\partial}{\partial y} - y\frac{\partial}{\partial x}\right) = \frac{\partial}{\partial\varphi}, \tag{C10}$$

which is Eq. (20).

APPENDIX D: DERIVATION OF TORQUE

The summation about M from $M = -\ell$ to ℓ in the torque Eq. (23) can be transformed from $M = 1$ to ℓ, i.e.,

$$\begin{aligned}\tau_z &= \sum_{\ell=0}^{\infty}\sum_{M=-\ell}^{\ell}\mathrm{i}M\frac{-4\pi G}{2\ell+1}Q_{\ell M}\tilde{q}_{\ell M}e^{-\mathrm{i}M\phi} \\ &= \sum_{\ell=1}^{\infty}\sum_{M=1}^{\ell}\frac{4\pi\mathrm{i}MG}{2\ell+1}\left[\tilde{q}_{\ell,-M}Q_{\ell,-M}e^{\mathrm{i}M\phi} - \tilde{q}_{\ell M}Q_{\ell M}e^{-\mathrm{i}M\phi}\right].\end{aligned} \tag{D1}$$

In consideration of the equation of spherical harmonics,

$$Y_{\ell,-M}(\theta,\varphi) = (-1)^M Y^*_{\ell M}(\theta,\varphi), \tag{D2}$$

there is a transformation relationship about the mass multipole moment or field,

$$\tilde{q}_{\ell,-M} = (-1)^M\tilde{q}^*_{\ell M}, \quad Q_{\ell,-M} = (-1)^M Q^*_{\ell M}, \tag{D3}$$

respectively. Hence, torque Eq. (D1) can be rewritten as

$$\tau_z = \sum_{\ell=1}^{\infty}\sum_{M=1}^{\ell}\frac{4\pi\mathrm{i}MG}{2\ell+1}\left[\tilde{q}^*_{\ell M}Q^*_{\ell M}e^{\mathrm{i}M\phi} - \tilde{q}_{\ell M}Q_{\ell M}e^{-\mathrm{i}M\phi}\right]. \tag{D4}$$

Substituting

$$\tilde{q}_{\ell M} = |\tilde{q}_{\ell M}|e^{\mathrm{i}\phi_{\tilde{q}_{\ell M}}}, \qquad Q_{\ell M} = |Q_{\ell M}|e^{\mathrm{i}\phi_{Q_{\ell M}}}, \tag{D5}$$

and

$$\begin{aligned}&e^{\mathrm{i}(-\phi_{\tilde{q}_{\ell M}}-\phi_{Q_{\ell M}}+M\phi)} - e^{\mathrm{i}(\phi_{\tilde{q}_{\ell M}}+\phi_{Q_{\ell M}}-M\phi)} \\ &\quad = -\mathrm{i}\left[2\sin\left(\phi_{\tilde{q}_{\ell M}} + \phi_{Q_{\ell M}} - M\phi\right)\right],\end{aligned} \tag{D6}$$

into Eq. (D4), one could obtain

$$\begin{aligned}\tau_z = \sum_{\ell=1}^{\infty}\sum_{M=1}^{\ell}&\frac{8\pi MG}{2\ell+1}|\tilde{q}_{\ell M}||Q_{\ell M}| \\ &\times\sin(\phi_{\tilde{q}_{\ell M}} + \phi_{Q_{\ell M}} - M\phi).\end{aligned} \tag{D7}$$

In the form of a matrix, it becomes

$$\begin{aligned}\tau_z = \sum_{\ell=1}^{\infty}\sum_{M=1}^{\ell}&\frac{8\pi MG}{2\ell+1}\begin{bmatrix}\mathrm{Re}[Q_{\ell M}] & \mathrm{Im}[Q_{\ell M}]\end{bmatrix} \\ &\times\begin{bmatrix}|\tilde{q}_{\ell M}|\cos\phi_{\tilde{q}_{\ell M}} & |\tilde{q}_{\ell M}|\sin\phi_{\tilde{q}_{\ell M}} \\ -|\tilde{q}_{\ell M}|\sin\phi_{\tilde{q}_{\ell M}} & |\tilde{q}_{\ell M}|\cos\phi_{\tilde{q}_{\ell M}}\end{bmatrix}\begin{bmatrix}\sin(-M\phi) \\ \cos(-M\phi)\end{bmatrix},\end{aligned}$$

which is Eq. (27).

[1] M. N. Nabighian, M. E. Ander, V. J. S. Grauch, R. O. Hansen, T. R. LaFehr, Y. Li, W. C. Pearson, J. W. Peirce, J. D. Phillips, and M. E. Ruder, Historical development of the gravity method in exploration, Geophysics **70**, 63ND (2005).

[2] E. H. van Leeuwen, BHP develops airborne gravity gradiometer for mineral exploration, Lead. Edge **19**, 1296 (2000).

[3] M. S. Zhdanov, E. Robert, and M. Souvik, Three-dimensional regularized focusing inversion of gravity gradient tensor component data, Geophysics **69**, 925 (2004).

[4] H. Rice, S. Kelmenson, and L. Mendelsohn, in *PLANS 2004. Position Location and Navigation Symposium (IEEE Cat. No. 04CH37556)* (IEEE, Monterey, California, 2004), p. 618.

[5] Z. Szabó, The history of the 125 year old Eötvös torsion balance, Acta Geod. Geophys. **51**, 273 (2016).

[6] D. DiFrancesco, A. Grierson, D. Kaputa, and T. Meyer, Gravity gradiometer systems – advances and challenges, Geophys. Prospect. **57**, 615 (2009).

[7] L. Völgyesi and Z. Ultmann, in *Geodesy for Planet Earth*, edited by S. Kenyon, M. C. Pacino, and U. Marti (Springer Berlin Heidelberg, Berlin, Heidelberg, 2012), p. 281.

[8] L. Völgyesi, G. Szondy, G. Tóth, G. Péter, B. Kiss, G. G. Barnaföldi, L. Deák, C. Égető, E. Fenyvesi, G. Gróf, L. Somlai, P. Harangozó, P. Levai, and P. Ván, in *Proceedings of International Conference on Precision Physics and Fundamental Physical Constants—PoS(FFK2019)* (Sissa Medialab, Tihany, Hungary, 2020), p. 041.

[9] H. Shaw and E. Lancaster-Jones, The Eötvös torsion balance, Proc. Phys. Soc. Lond. **35**, 151 (1922).

[10] It is opposite direction defined in Ref. [9].

[11] E. Fischbach and C. L. Talmadge, *The Search for Non-Newtonian Gravity* (Springer, New York, 1999).

[12] J. D. Jackson, *Classical Electrodynamics* (Wiley, New York, 1999).

[13] C. C. Speake, G. D. Hammond, and C. Trenkel, The torsion balance as a tool for geophysical prospecting, Geophysics **66**, 527 (2001).

[14] E. G. Adelberger, C. W. Stubbs, B. R. Heckel, Y. Su, H. E. Swanson, G. Smith, J. H. Gundlach, and W. F. Rogers, Testing the equivalence principle in the field of the Earth: Particle physics at masses below 1 μeV?, Phys. Rev. D **42**, 3267 (1990).

[15] D. A. Varshalovich, A. N. Moskalev, and V. K. Khersonskii, *Quantum Theory of Angular Momentum* (World Scientific Pub, Singapore, 1988).

[16] Here the derivation of the gravitational torque is completely different from that in Ref. [14].

[17] K.-Y. Choi, *A new equivalence principle test using a rotating torsion balance*, Ph.D. thesis, University of Washington, Seattle, 2006.

[18] L. Zhu, Q. Liu, H.-H. Zhao, Q.-L. Gong, S.-Q. Yang, P. Luo, C.-G. Shao, Q.-L. Wang, L.-C. Tu, and J. Luo, Test of the equivalence principle with chiral masses using a rotating torsion pendulum, Phys. Rev. Lett. **121**, 261101 (2018).